

Convolution based hybrid image processing technique for microscopic images of etch-pits in Nuclear Track Detectors

Kanik Palodhi, Joydeep Chatterjee

Department of Applied Optics and Photonics, University of Calcutta, Kolkata 700106, India

Rupamoy Bhattacharyya¹, S. Dey, Sanjay K. Ghosh, Atanu Maulik, Sibaji Raha

Centre for Astroparticle Physics and Space Science, Bose Institute, Kolkata 700 091, India

Abstract

A novel image processing technique based on convolution is developed for analyzing the etch-pit images in Nuclear Track Detectors (NTDs). Promising results have been obtained for both identifying and counting the etch-pits in the NTDs. Such method establishes itself to be the first of its kind to have been applied successfully to NTDs.

Keywords: Nuclear Track Detector, Etch-pit, Image processing, Image convolution

1. Introduction

Nuclear Track Detectors (NTDs) have been used in charged particle detection for many decades in fields ranging from physics to geology [1, 2]. NTDs are dielectric solids (e.g., polymer films of thickness $\sim 100 \mu\text{m}$). A charged particle while passing through the NTD material, loses energy by ionizing the medium. If the energy loss is above a certain threshold, then the particle leaves behind a permanent damage trail, essentially broken polymer chains in case of plastics,

¹Corresponding author.

E-mail address: rupamoy@gmail.com(Rupamoy Bhattacharyya)

Present address: Indian Institute of Science Education and Research Bhopal, Bhopal, India

called a “latent track”. Obviously, this threshold will be different for different NTD materials. Such damaged regions become chemically more reactive compared to the undamaged bulk material. When such an NTD containing any *latent track* is treated with a suitable chemical reagent, called etchant, materials along the damage trail is etched out at a much faster rate compared to the surrounding bulk material, resulting in etch pits large enough (of the order of micron) to be observed under optical microscopes. The geometry of such etch-pits can reveal crucial information on the identity of the particles forming such tracks. Because of their low cost, ease of handling and existence of natural thresholds of registration (which helps in reducing the background), NTDs are often the detectors of choice in the search for rare heavily ionizing hypothesized particles (e.g., magnetic monopoles, strangelets) in cosmic rays as well as particle accelerators [3, 4]. It may be mentioned here we are aiming to use a low cost, commercially available polymer, identified as Polyethylene Terephthalate (PET), as NTD in the search for strangelets through the deployment of large-area arrays at mountain altitudes [5].

In such searches employing NTDs, the task of scanning of etched NTDs to locate the etch-pit openings on their surface is extremely labour intensive as the researchers are required to scan large areas of NTDs under high magnification. The difficulty of finding a track due to any rare event is compounded by the presence of background which can come from other ionizing radiations and also from structural defects in the plastic which creeps in during the polymerization process. Therefore, challenges of rare event search with NTDs are primarily technological as the conventional image analysis software coming up short in the task of track identification.

In this paper, we are proposing a novel approach for etch-pit image identification and counting in NTDs, which shows much-improved performance compared to more “classical” (employing cuts based on just grey level, size, etc.) approaches to image analysis.

2. Experimental technique

This section describes the image analysis techniques that are applied to the unprocessed surface images of exposed and etched NTDs, captured by QWin software using a Leica DM4000B optical microscope. The etch-pits appear dark as compared to the background of NTD surface; however, the challenge is to separately recognize them from the other artifacts generated during chemical etching and scratches and defects, which also appear dark, as shown in Fig 1. For this study, we have used the etch-pit images from Columbia Resin #39 (CR-39) and Polyethylene terephthalate (PET) NTDs exposed to cosmic rays at high mountain altitudes [5] and heavy ions from accelerators [6].

The image analysis technique that we have applied here is based on sequential application of blind deconvolution and convolution with a suitable mask size obtained from the analysis of the area occupied by the opening of an etch-pit. Before going to the application of the technique, few considerations regarding image quality and acquisition are described below:

Typical size of etch-pit openings are roughly $\sim \mu\text{m}$. As mentioned earlier, there are similar types of artifacts of the similar area which may be wrongly counted. Convolutions with the original size of the etch-pits, therefore, need to be augmented with the shape of the pit-openings. It is known that the typical shape of the opening of the etch-pits will be elliptical, and in special cases circular (for normal incidence of the incoming ion), as shown in Fig.5 and Fig.4 respectively.

First of all, among all the present etch-pits, the biggest one in shape and size is ascertained, and a similar convolution circular mask is formed which is convolved with the entire etch-pit image. As discussed, it provides a huge advantage since the convolution peak, generated at the centre of the pit, helps to determine the position of a track. If any of the etch-pit openings within the captured image can be expressed as $N(x, y)$, considering its 2D form and the circular mask, mentioned above is expressed as $M(x, y)$, then their convolution

can be written as

$$f_c(x, y) = \iint_{-\infty}^{+\infty} N(x - x_0, y - y_0) M(x_0, y_0) dx_0 dy_0 \quad (1)$$

The above expression is commonly written as $f_c(x, y) = N(x, y) \times M(x, y)$ and is routinely used in different domains of optics and signal processing [7]. The advantage of using convolution is that in case of circular mask convolving with circular or elliptical opening of etch-pits, the peak values are produced at the centre provided that the shapes and sizes are nearly equal. This is true for NTDs since the average diameter of the tracks for the cases shown here correspond to nearly 120 pixels ($\sim 12 \mu\text{m}$). This is illustrated in a simulation shown in Fig.2 where a one-dimensional representation of convolution is shown between a pit and a mask of the same size. In 1D representation, the functions are represented with a single variable provided in terms of pixels with an analogy to the images. Therefore, when $N(x)$ (Fig.2(a)), essentially a one-dimensional projection of etch-pit profile, gets convolved with the mask $M(x)$ (Fig.2(b)). The result is a well-known triangular function as shown in Fig.2(d) with a dotted line.

For actual cases in NTDs however, the other artifacts or the scratches are of different shapes and sizes, will result in similar convolution peaks. Therefore, for enhancing the peak values near the centres of etch-pits, a deconvolution process with a Gaussian mask as shown in Fig.2(c) of similar shape (half-width ~ 120 pixels) is introduced [8]. This provides higher peaks compared to simple convolution for definitive shapes of NTDs as shown in Fig.2(d). Theoretically, this can be represented considering a Fourier domain explanation where $G(x)$ (Fig.2(c)) is a 1D representative Gaussian function centred at origin given by

$$G(x) = \exp(-ax^2) \quad (2)$$

The Fourier transform of the above Gaussian function, also a Gaussian function is written in terms of spatial frequency along X-direction k_x , can be written as

$$F(G(x)) = \hat{\mathbf{G}}(k_x) = \sqrt{\frac{\pi}{a}} \exp\left(\frac{-\pi^2 k_x^2}{a}\right) \quad (3)$$

Therefore, deconvolution in Fourier domain can be expressed as

$$\hat{\mathbf{f}}_d(k_x) = \frac{\hat{\mathbf{N}}(k_x)}{\hat{\mathbf{G}}(k_x)} \quad (4)$$

where $\hat{\mathbf{f}}_d(k_x)$ and $\hat{\mathbf{N}}(k_x)$ represent the Fourier transforms of the respective functions introduced already. As described in Ref. [8], the technique of applying Gaussian in deconvolution reduces a lot of problems since the characters of the functions in both domains are well-known [8]. Next, inverse Fourier transform is applied to Eq. (4) and can be expressed as in terms of convolution

$$f_d(x) = \frac{N(x)}{G(x)} \quad (5)$$

After obtaining this, another convolution operation with the standard circular mask described previously (in its 1D representation) is performed to enhance the peak at the centre of the etch-pit as shown in Fig.2(d). This is expressed in terms of convolution operator as

$$f_{dc}(x) = f_d(x) \times M(x) \quad (6)$$

A comparison is shown in Fig.3(d) clearly shows that $f_{dc}(x)$, function due to Gaussian deconvolution followed by convolution (Eq. (6)) with mask produces higher peaks compared to simple convolution operation represented by $f_c(x)$. Without any loss of generality, the two-dimensional simulation results corresponding to the above operations are presented in Fig.3, where the effects of shape variations of etch-pit openings are also considered.

In the case of actual microscopic NTD surface images, the background being whitish, the dark etch-pits have a significantly higher signal to noise ratio where this operation produces a better result. Another advantage is that in cases of noise removal of corresponding frequency domain processing can be done since the convolution process lends itself easily to convolution and deconvolution.

3. Image analysis and results

The novel image analysis technique employed here is tested with multiple microscopic images of NTDs using the copyrighted software Cell Counter [9].

Images of etch-pits from	Manual count	Automated count	Percentage error
Accelerator exposure	301	302	0.33%
Open-air exposure	152	147	3.3%

Table 1: Results of the manual and automatic counts of etch-pits on 58 and 53 images of accelerator exposed PET and open-air exposed CR-39 films respectively.

As described before, images of etch-pits due to accelerator exposed NTDs (Fig.4 and Fig.5) are often used as reliable guidance. Fig.4(a) shows an image frame, with a normal incidence of ions from accelerator; the image has multiple defects and scratches, even of sizes similar to that of the actual etch-pits. Clearly, the etch-pits has been separated from the rest and counted (as well as marked) correctly as shown in Fig.4(b).

Fig.5(a) shows the images of etch-pits for accelerator exposed NTDs (angle of incidence of the beam is 30°) with elliptical openings. The figure is, as usual, riddled with different types of defects. The same algorithm is used here as before, which yields surprisingly good results even in the overlapped region near the bottom of the Fig.4(b).

Finally, in Fig.6(a), NTD surface image from open-air exposure at Darjeeling is presented. It can be seen, the background defects in this case are more prominent compared to those found in Fig.4 and Fig.5. The roughening of the NTD surface is expected as the films were given open-air exposure. In this case too, most of the tracks are rightly recognized but the one at the bottom left side as shown in Fig.6(b). This is a track generated by a cosmic ray with a very high angle of incidence. We have examined hundreds of similar samples and in most cases, almost all the etch-pits are identified making error percentage extremely small as given in Table 1.

4. Comparison with other methods

Any shape detection algorithm such as Hough transform or shape fitting etc. works for a definite shape. Even if there are slight deviations from the actual shape, most of these algorithms fail to detect the shape. In the present case, etch-pits can be both circular and elliptical but with wide variations. Our attempts with conventional image analysis methods didn't yield any good result. These techniques can't be easily used for counting without morphological techniques as well. Contrary to conventional methods, using the proposed convolution method, the detection of a peak at the location of the etch-pits is much better and simultaneously provides its coordinates. The proposed method is simpler yet more robust than some well-known shape detecting algorithms like Hough Transform, morphological operations, watershed segmentation [10, 11, 12] etc. A few other advantages are listed below:

- No simultaneous frequency domain processing is required for this technique.
- Even at the overlapping regions of two or more etch-pits, which are difficult to handle with other image analysis methods, tracks can be easily recognized and counted by this technique.

5. Conclusion

A novel image analysis technique based on convolution is shown to generate much better results compared to many other techniques for etch-pit detection in NTDs. It promises to substantially speed up the task of track identification and analysis, which is the chief technical challenge for any experiments employing large area NTD arrays.

Acknowledgments

Authors are grateful to Dr. Debapriyo Syam for many useful discussions. KP and JC wish to acknowledge TEQIP-III, University of Calcutta and Depart-

ment of Applied Optics and Photonics, University of Calcutta. RB wishes to acknowledge Project No. SERB/PHY/2016/041 and SB/S2/RJN-29/2013 for financial support. This work is partially funded by IRHPA (Intensification of Research in High Priority Areas) Project (IR/S2/PF-01/2011 dated 26.06.2012) of the Science and Engineering Research Council (SERC), DST, Government of India, New Delhi.

References

References

- [1] R. L. Fleischer, P. B. Price, R. M. Walker, Nuclear Tracks in Solids. Principles and Applications, University of California Press, Berkeley, 1975.
- [2] Nuclear track detectors in astroparticle and nuclear physics, Radiation Measurements 43 (2008) S144 – S150, proceedings of the 23rd International Conference on Nuclear Tracks in Solids. doi:<https://doi.org/10.1016/j.radmeas.2008.04.061>.
- [3] The MoEDAL collaboration, B. Acharya, J. Alexandre, K. Bendtz, P. Benes, J. Bernab  , M. Campbell, S. Cecchini, J. Chwastowski, A. Chatterjee, M. de Montigny, D. Derendarz, A. De Roeck, J. R. Ellis, M. Fairbairn, D. Felea, M. Frank, D. Frekers, C. Garcia, G. Giacomelli, D. Hasegan, M. Kalliokoski, A. Katre, D.-W. Kim, M. G. L. King, K. Kinoshita, D. Lacarr  re, S. C. Lee, C. Leroy, A. Lioni, A. Margiotta, N. Mauri, N. E. Mavromatos, P. Mermod, D. Milstead, V. A. Mitsou, R. Orava, B. Parker, L. Pasqualini, L. Patrizii, G. E. P  v  las, J. L. Pinfold, M. Platkevi  , V. Popa, M. Pozzato, S. Pospisil, A. Rajantie, Z. Sahnoun, M. Sakellariadou, S. Sarkar, G. Semenoff, G. Sirri, K. Sliwa, R. Soluk, M. Spurio, Y. N. Srivastava, R. Staszewski, M. Suk, J. Swain, M. Tenti, V. Togo, M. Trzebinski, J. A. Tuszyński, V. Vento, O. Vives, Z. Vykydal, T. Whyntie, A. Widom, G. Willems, J. H. Yoon, Search for magnetic

- monopoles with the moedal prototype trapping detector in 8 tev proton-proton collisions at the lhc, *Journal of High Energy Physics* 2016 (8) (2016) 67. doi:10.1007/JHEP08(2016)067.
- [4] S. Balestra, S. Cecchini, M. Cozzi, M. Errico, F. Fabbri, G. Giacomelli, R. Giacomelli, M. Giorgini, A. Kumar, S. Manzoor, J. McDonald, G. Mandrioli, S. Marcellini, A. Margiotta, E. Medinaceli, L. Patrizzii, J. Pinfold, V. Popa, I. E. Qureshi, O. Saavedra, Z. Sahnoun, G. Sirri, M. Spurio, V. Togo, A. Velarde, A. Zanini, Magnetic Monopole search at high altitude with the SLIM experiment, *Eur. Phys. J. C* 55 (2008) 57–63. arXiv:0801.4913, doi:10.1140/epjc/s10052-008-0597-3.
- [5] R. Bhattacharyya, S. Dey, S. K. Ghosh, A. Maulik, S. Raha, D. Syam, Study of radiation background at various high altitude locations in preparation for rare event search in cosmic rays, *Journal of Cosmology and Astroparticle Physics* (04) (2017) 035. doi:10.1088/1475-7516/2017/04/035.
- [6] S. Dey, A. Maulik, S. Raha, S. K. Saha, D. Syam, Particle identification with polyethylene terephthalate (pet) detector with high detection threshold, *Nuclear Instruments and Methods in Physics Research Section B: Beam Interactions with Materials and Atoms* 336 (2014) 163 – 166. doi:https://doi.org/10.1016/j.nimb.2014.07.006.
- [7] J. D. Gaskill, *Linear Systems, Fourier Transforms, and Optics*, Wiley-Interscience.
- [8] W. Ulmer, Convolution/deconvolution of generalized gaussian kernels with applications to proton/photon physics and electron capture of charged particles, *Journal of Physics: Conference Series* 410 (2013) 012122. doi:10.1088/1742-6596/410/1/012122.
- [9] J. Chatterjee, S. Chakraborty, K. Palodhi, Cell counter [computer software] (SW-12248/2019 22 Feb 2019).

- [10] V. Piuri, F. Scotti, Morphological classification of blood leucocytes by microscope images, in: 2004 IEEE International Conference on Computational Intelligence for Measurement Systems and Applications, 2004. CIMSA., 2004, pp. 103–108. doi:10.1109/CIMSA.2004.1397242.
- [11] J. M. Sharif, M. F. Miswan, M. A. Ngadi, M. S. H. Salam, M. M. bin Abdul Jamil, Red Blood Cell Segmentation Using Masking and Watershed Algorithm: A Preliminary Study, International Conference on Biomedical Engineering (ICoBE).
- [12] F. Zana, J. C. Klein, A multimodal registration algorithm of eye fundus images using vessels detection and hough transform, IEEE Transactions on Medical Imaging 18 (5) (1999) 419–428. doi:10.1109/42.774169.

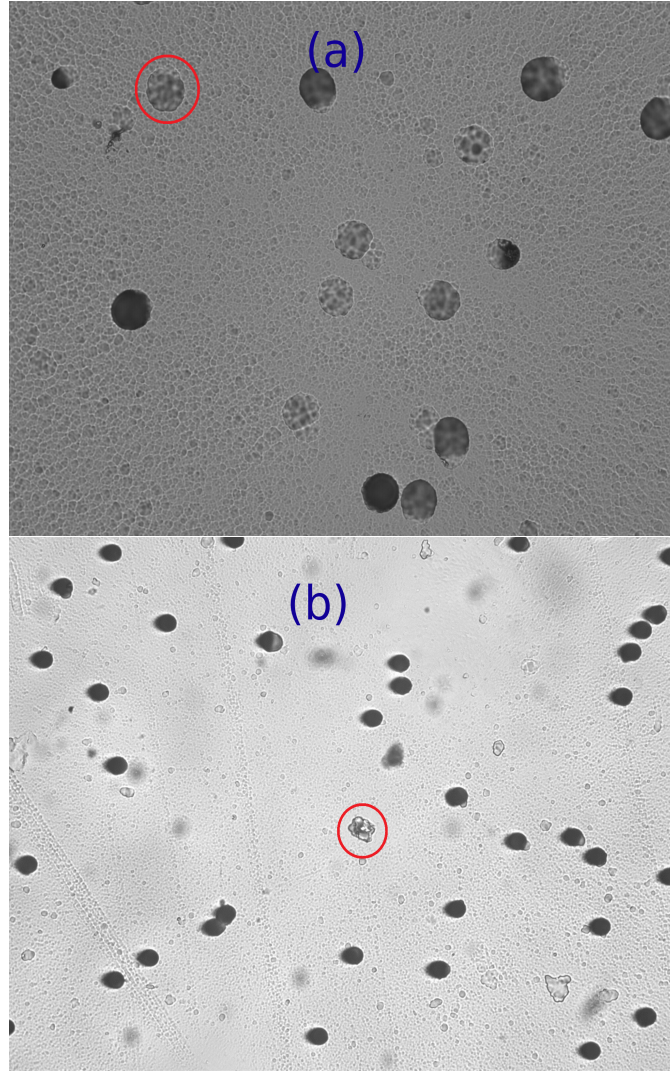


Figure 1: Microscopic surface images of (a) CR-39 (NTD) exposed to open-air at Darjeeling, India and (b) PET (NTD) exposed to ^{32}S ions from accelerator. Typical scratches and/or other defects are shown inside red circle. It may be noted here that the surface quality of the NTDs which get open-air exposure are worsened due to harsh environmental conditions.

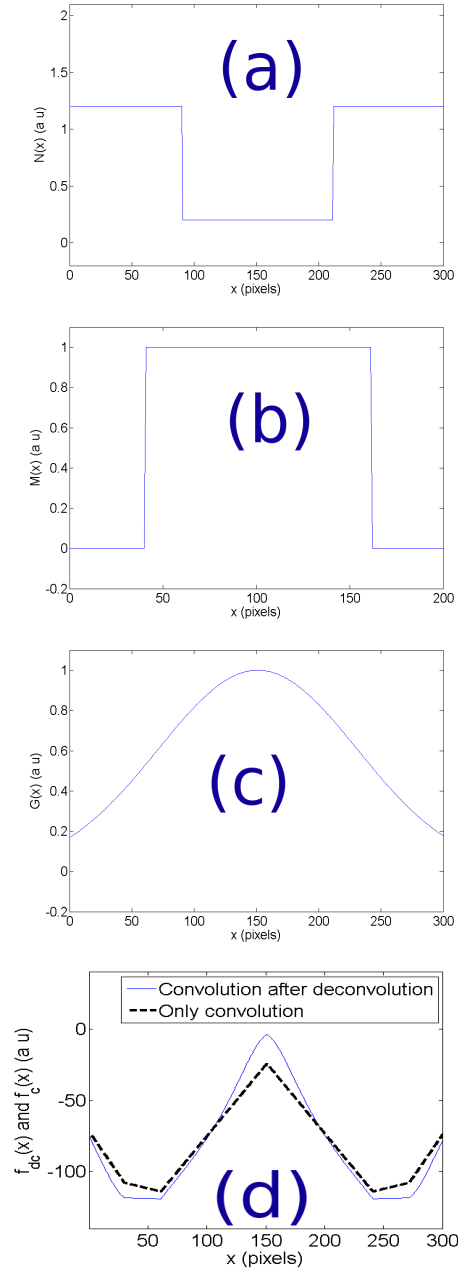


Figure 2: One dimensional representation of only convolution and then deconvolution followed by convolution process. (a) 1D representation of etch-pit profile $N(x)$ (width ~ 120 pixel); (b) The circular mask $M(x)$ (width ~ 120 pixels); (c) The Gaussian mask used in deconvolution $G(x)$ (half-width ~ 120 pixels); (d) Comparison of convolution $f_c(x)$ and deconvolution followed by convolution $f_{dc}(x)$.

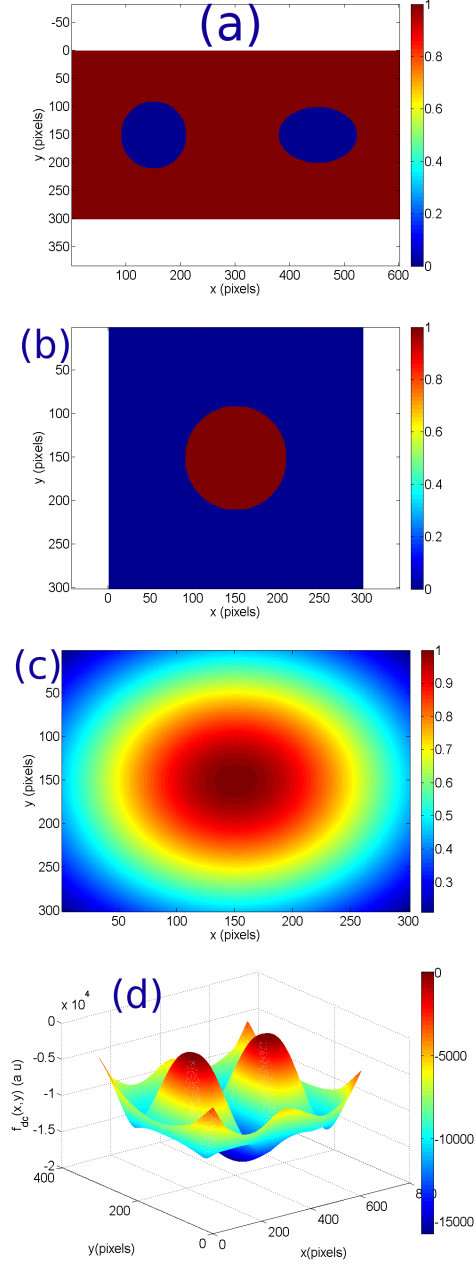


Figure 3: Two dimensional representation of only convolution and then deconvolution followed by convolution process. (a) Etch-pits of both circular and elliptical shape (diameter ~ 120 pixel); (b) The circular mask(diameter ~ 120 pixels); (c) The Gaussian mask used in deconvolution (half-width ~ 120 pixels); (d) Deconvolution followed by convolution $f_{dc}(x)$.

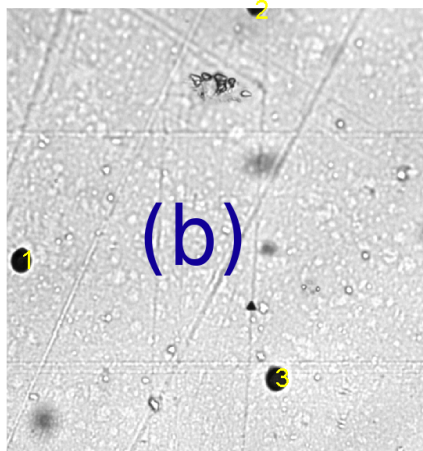
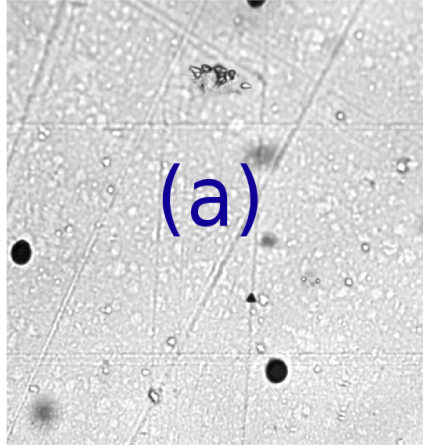


Figure 4: (a) Etch-pits due to normally incident ions. This image also shows scratches (dark as compared to the whitish background); (b) Judicially counting of etch-pits among multiple types of defects. The etch-pits are correctly identified from the background.

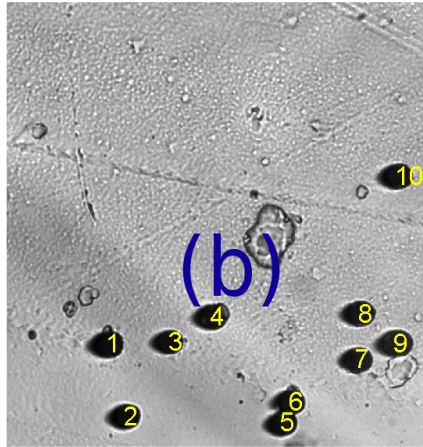
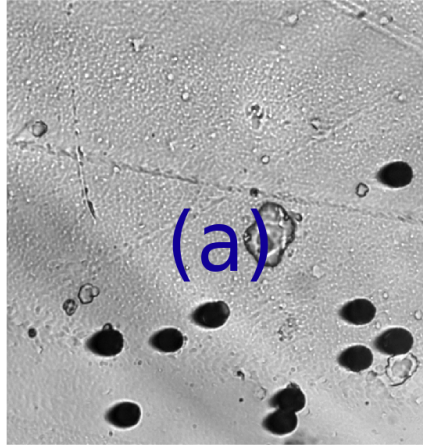


Figure 5: (a) Etch-pits due to the ions striking at 30° angle of incidence, showing darker etch-pits and defects or scratches; (b) Counting of etch-pits separately from multiple types of defects.

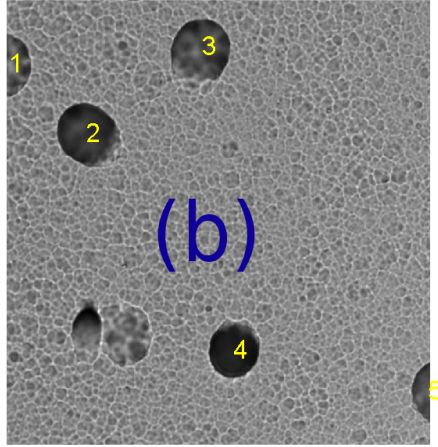
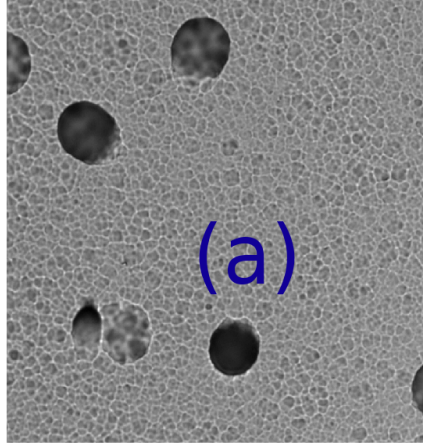


Figure 6: (a) Etch-pits due to charged particles with different angle of incidences on CR-39 (NTD) exposed to open-air at Darjeeling, India.; (b) Counting of etch-pits separately from multiple-type of defects while missing one with very high incident angle.